Available online at www.sciencedirect.com

ScienceDirect

Procedia Manufacturing 6 (2016) 45 – 52

Procedia MANUFACTURING

16th Machining Innovations Conference for Aerospace Industry - MIC 2016

# Automated dressing of graphite electrodes for electrical discharge machining (EDM) of seal slots in turbine components

Eckart Uhlmann[a,b]; David C. Domingos[a,]*

[a]*Fraunhofer Institute for Production Systems and Design Technology IPK, Pascalstrasse 8-9, 10587 Berlin, Germany*
[b]*Institute for Machine Tools and Factory Management IWF, Technische Universität Berlin, Pascalstrasse 8-9, 10587 Berlin, Germany*

**Abstract**

The die-sinking EDM is applied in the aerospace industry for the machining of seal slots in blades and in structural components made of nickel-base alloys, normally applying graphite electrodes. The objective of this work was the development of a technology to dress the graphite electrodes inside the EDM machine tool, with the aim of rebuilding the original shape of the worn electrodes between EDM cycles. The milestones consisted on (I) understanding the wear behavior of the electrodes while machining the slots, (II) the development of the dressing technology applying the DoE-method and determination of statistically high influencing parameters, and finally (III) the integration of the dressing technology into the process chain.


Peer-review under responsibility of the NAMRI Scientific Committee

*Keywords:* die-sinking EDM; dressing of electrodes; nickel-base alloy; turbine components; process automation.

## 1. Introduction

The high demands on next generation aero engines, with challenging targets for $CO_2$, NOx and noise emissions according to CLAIRE (technology program *Clean Air Engine* from MTU Aero Engines, Germany), push new technological developments such as the application of new materials and new manufacturing technologies as well as the development of automated process chains [1, 2]. The fabrication of seal slots in blades and further components in the aerospace industry is usually carried out by die-sinking EDM. Latest developments to improve this

* Corresponding author. Tel.: +49 (0) 30 39006-413; fax: +49 (0) 30 3911037.
*E-mail address:* david.carlos.domingos@ipk.fraunhofer.de


Peer-review under responsibility of the NAMRI Scientific Committee
doi:10.1016/j.promfg.2016.11.007

manufacturing step focused on reducing the machining times and relative wear of electrodes through process optimization as well as on the development of the vibration-assisted EDM-technology [3, 4, 5, 6]. The current work focuses on the automation of the EDM of seal slots, by means of dressing the tool electrodes inside the machine tool, thereby eliminating a further manipulation of the electrodes by the machine operator.

## 2. Machine tool and materials

The machine tool GENIUS 1000 from company Zimmer&Kreim and the dielectric fluid IME-MH from company Oelheld were applied for conducting the experimental investigations on die-sinking EDM of seal slots and on dressing of the worn graphite electrodes.

Two distinct graphite electrode materials were applied in the EDM of the seal slots in turbine components: ultrafine graphite EDM-3 from company Poco Graphite Inc., USA, and ultrafine graphite HK-6 from company Tokai Carbon Co. Ltd., Japan. Both materials find application in the aerospace industry, are isotropic and ultrafine graphite (1 µm – 5 µm) according to their primary particle sizes prior to the forming, coking and graphitization processes. The main physical properties of both graphite types are presented in Table 1.

Table 1. Physical properties of the graphite electrodes [7, 8].

| Physical Properties | EDM-3 | HK-6 |
|---|---|---|
| Density ρ [g cm$^{-3}$] | 1.81 | 1.86 |
| Average particle size [µm] | < 5 | 3 |
| Specific electrical conductivity $\sigma_0$ (273,15 K) [m S mm$^{-2}$] | 0.064 | 0.083 |
| Specific electrical resistance ρ [µ Ω m] | 15.6 | 12 |
| Hardness [Shore A] | 73 | 68 |

The nickel-base casting alloy MAR-M247 was chosen as workpiece material for the experiments, as this is considered a very important Ni-base material for the turbomachinery industry [6], finding many applications there. The alloy went through a hot-isostatic-pressing (HIP) process followed by a heat treatment [9], possess a density ρ = 8.54 g/cm3, a hardness given in Rockwell C ranging between 30 < HRC < 40, and a melting point between $T_m$ = 1,315 °C and $T_m$ = 1,340 °C [10]. The SEM-images in Fig. 1 present the conventional casting polycrystalline microstructure and the concentration of the carbides at the grain boundaries, resulted from the HIP process. Further carbides are also solidified within the γ-matrix. The γ-matrix is brighter and possess a net-like mesh form, while the dark γ'-phase is placed inside this matrix. The most available elements of the alloy can be identified at the EDX-analysis of the overall sample, which are Ni, Co, Cr, W and Al.

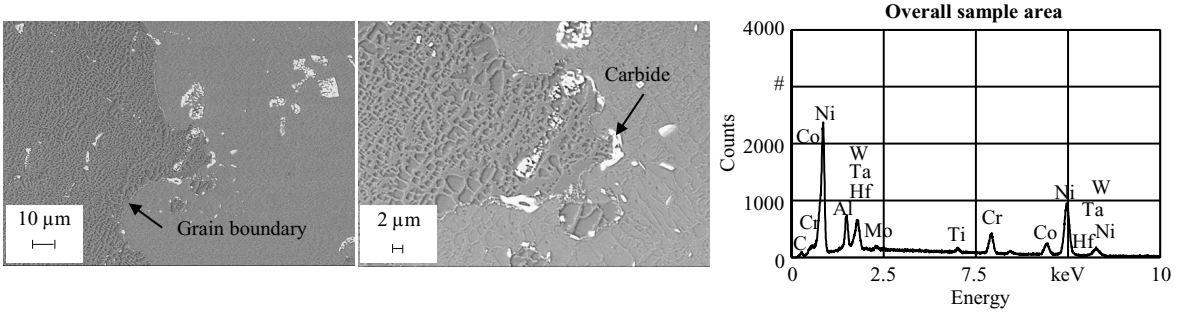


Fig. 1. Metallographic and energy dispersive X-ray (EDX) analyses of the applied nickel-base casting alloy MAR-M247.

A total of four materials were selected and applied as dressing plates in the experiments, being two metallic and two graphite materials. The materials applied as dressing plates were the following: ultrafine graphite EDM-3, copper infiltrated graphite EDM-C3 (Poco), fine grained cemented carbide CF-H40S (Ceratizit) and ordinary brass CuZn36. The main physical properties of these materials are presented in Table 2, considering their application as electrodes at EDM.

Table 2. Physical properties of the applied dressing plates [9].

| Physical Properties | EDM-C3 | CuZn36 | CH-H40S |
|---|---|---|---|
| Average particle size [µm] | < 5 | 15 - 30 | 0.8 - 2.5 |
| Specific electrical conductivity $\sigma_0$ (273.15 K) [m S mm$^{-2}$] | 0.3125 | 15.15 | 18.87 |
| Thermal conductivity λ (273.15 K) [W m-1 K-1] | > 110 | 120 | 90 |
| Melting point / Sublimation point* [K] | 3350* | 920 | 2860 |

## 3. Development of the dressing technology

### *3.1. Description of the dressing process*

Commonly, in the die-sinking EDM, the tool electrodes are fixed to the mandrel of the machine tool, while the workpieces to be processed are clamped on the machine table. The material removal rate $V_W$ thus describes the volume of material removed from the workpiece per time unit, the workpiece being in the present study the MAR-M247 plates. The electrode wear rate $V_E$ describes the volume of material removed from the tool electrode per time unit, meaning the volume removed from the applied graphite electrodes fixed on the mandrel. By the end of the EDM process, the cavities in the MAR-M247 workpieces are produced and the electrodes present a tool wear, which can be measured especially on the corners and frontally. The EDM process (right) and the wear pattern of the tool electrodes (left) are presented in Fig. 2.

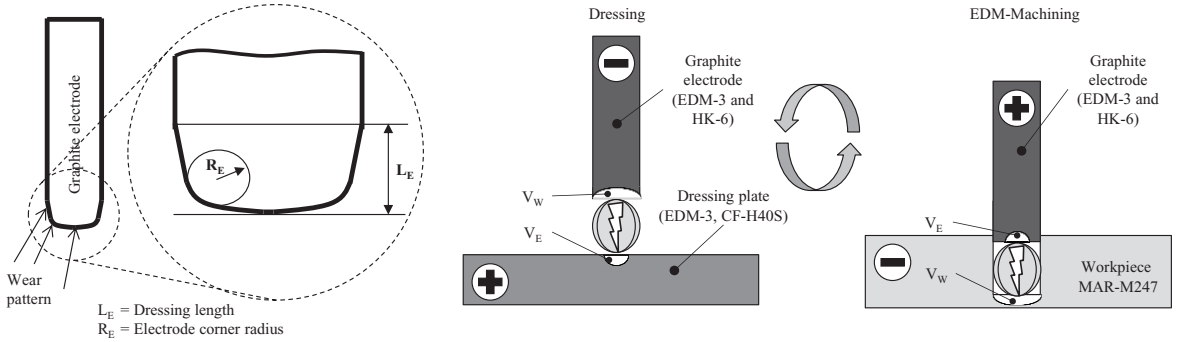


Fig. 2. Schematic representation of the wear of graphite electrodes and of the EDM and dressing processes.

During the deployment of the dressing technology the described set-up becomes the opposite, because the process now focuses on removing material from the former tool electrodes, which are fixed to the mandrel of the machine. The former graphite electrodes become thus the workpieces to be machined. On the other hand, the dressing plates fixed to the machine table constitute the tool electrodes during the dressing process. By performing this development, the polarity of the machine mandrel has to become negative. Although the definitions for material removal rate $V_W$ and tool wear rate $V_E$ continue unmodified with this set-up, the $V_W$ now refers to the volume of material removed from the former electrodes fixed on the mandrel, while $V_E$ refers to the volume of material removed from the dressing plates (Fig. 2).

### *3.2. Wear pattern development of graphite electrodes and technological boundary conditions*

The development of the dressing technology based on the definition of the boundary conditions regarding the wear pattern development of graphite electrodes after subsequently EDM cycles. The die-sinking EDM of the seal slots was conducted applying a previous developed technology, and the main EDM parameters are presented in Fig. 3. The diagram shows that the corner radius of electrode $R_E$ continuously increased by increasing the number of EDM cycles, especially due to the fact that the electrical discharges spark in the region with the highest electric field enhancement, e.g. electrode corner radiuses. This wear behavior helped to determine the minimal dressing length

$L_{E,min}$ necessary to rebuild the original shape of the electrodes, which should be at least as long as the electrode radius $R_E$ after one machining cycle. Therefore the value $L_{e,min}$ = 600 µm was set as boundary condition. In order to avoid waste of graphite electrodes, the maximum frontal dressing length of the electrodes was set $L_{E,max}$ = 800 µm. The dressing time t should be as short as possible (t < 4 min), with the aim of implementing the technology in a production chain. The error bars in all figures of this paper refer to the standard deviation of the measurements.

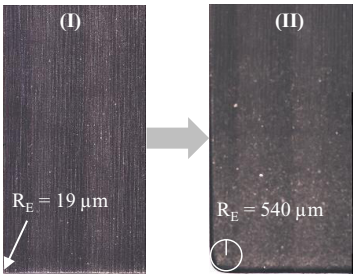


Electrode corner radius $R_E$ before (I) and after (II) EDM-machining

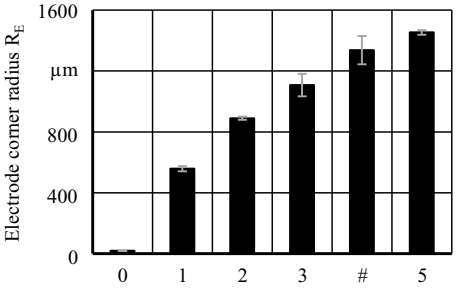


**Process parameters:**
$i_e$ = 29 A; $\hat{u}_i$ = 270 V
$t_i$ = 32 µs; $t_0$ = 14 µs
Polarity of electrode: +
Machining depth: s = 11 mm
**Tool electrode:**
EDM-3 / Number of electrodes: 12
Electrode frontal area: $A_E$ = 89.6 mm²
**Workpiece:** MAR-M247
**Dielectric fluid:** IonoPlus IME-MH

Fig. 3. Development of the corner radius of electrodes $R_E$ after subsequently EDM cycles.

### *3.3. Analysis of distinct dressing plate materials*

The first analysis comprised the comparison of the four distinct materials applied as dressing plates, by means of understanding the influence of dressing process parameters and of the materials on the dressing process. Four dressing process parameters were varied in the experiments for each dressing plate material, and the levels for the process parameters are presented in Table 3, together with the best results achieved for each material. The dressing parameters applied to achieve the mentioned best results are signed bold. Brass CuZn36 did not reach the set $L_{e,min}$ = 600 µm due to the high wear of this dressing plate, which can be led back to the low melting point of brass. The cemented carbide CF-H40S presented good results for the dressing technology and one parameter set tested was able to fulfill all requirements on process outputs, with dressing length $L_E$ > 600 µm, material removal rate $V_W$ = 15.8 mm³/min and short machining time t = 3.5 min. The low wear of the dressing plate made of cemented carbide, which is confirmed by the high frontal dressing length $L_E$ achieved on the electrodes, is a result of a combination of low specific electrical resistivity of the bonding material cobalt and the high sublimation point of tungsten carbide [11]. Both the discharge current $i_e$ and the erosion time between flushing intervals $t_{ero}$ possess a high significant influence on at least two process outputs, enabling the further optimization of the dressing process; the influence of the pulse duration $t_i$ and pulse interval time $t_0$ on process outputs was statistically indifferent. These results described here deal with the development of the dressing technology applying CF-H40S as dressing plate.

Table 3. Levels for the dressing process parameters and best results.

| Dressing plate material | $t_i$ [µs] | | $t_0$ [µs] | | $i_e$ [A] | | $t_{ero}$ [s] | | t [min] | $V_W$ [mm³/min] | $L_E$ [µm] |
|---|---|---|---|---|---|---|---|---|---|---|---|
| | + | - | + | - | + | - | + | - | | | |
| **EDM-3** | **75** | 56 | **56** | 42 | 14.8 | **8.3** | **2** | 0.5 | **4.9** | **13.3** | **722** |
| **EDM-C3** | **100** | 75 | 56 | **42** | 14.8 | **10.8** | **2** | 0.5 | **3.5** | **15.3** | **604** |
| **CuZn36** | 320 | **240** | 240 | **180** | **8.3** | 4.0 | **2** | 0.5 | **3.0** | **11.4** | **371** |
| **CF-H40S** | **320** | 240 | 240 | **180** | 14.8 | **10.8** | **2** | 0.5 | **3.5** | **15.8** | **614** |

### *3.4. Technology optimization with full-factorial experimental design*

A full-factorial analysis of the influence of the discharge current $i_e$ and erosion time between flushing intervals $t_{ero}$ on process outputs applying cemented carbide as dressing plate are presented in Fig. 4. The material removal rate $V_W$, frontal dressing length $L_E$ and electrode wear rate $V_E$ are displayed in the figure. The raise of the discharge current $i_e$ guides towards an increase of the material removal rate $V_W$, decrease of the frontal dressing length $L_E$ and

increase of the electrode wear rate $V_E$, as a result of higher discharge energy available [11]. The steep increase of the electrode wear rate $V_E$ with increasing discharge current $i_e$ leads to the reduction of the frontal dressing length of the graphite electrode. The best results with CF-H40S towards the fulfillment of the defined boundary conditions were achieved with a discharge current $i_e$ = 10.8 A and erosion time between flushing intervals $t_{ero}$ = 4.0 s. This technology led to a material removal rate $V_W$ = 14.92 mm³/min, a frontal dressing length $L_E$ = 594 µm and a machining time t = 3.57 min. The difference between the results achieved at 3.3 and 3.4 is due to the fact that the electrodes applied during the experimentation at 3.3 were worn electrodes ($R_E$ > 600 µm), while nearly sharp electrodes ($R_E$ < 600 µm) were applied at 3.4.

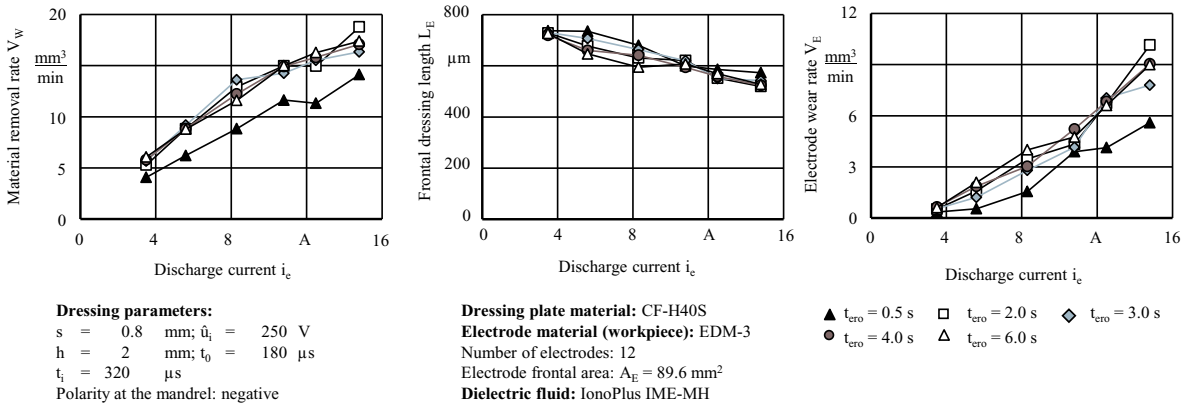


Fig. 4. Influence of discharge current $i_e$ and erosion time between flushing intervals $t_{ero}$ on the dressing results.

### *3.5. Influence of electrode material on the dressing process*

The dressing technologies developed so far considered only the application of electrode materials made of graphite EDM-3. At this stage, this technology was extended for dressing graphite electrodes made of the material HK-6, which was also used as electrode material for producing the high aspect ratio cavities in MAR-M247. The machining depths studied were s = 0.8 mm, s = 0.9 mm and s = 1.0 mm and the results are presented in Fig. 5. The machining time t and the frontal dressing length $L_E$ increase linearly with the rising machining depths s, both for graphite electrodes made of EDM-3 and HK-6, showing the stability of the dressing process while machining with relative small machining depths s. The material removal rate $V_W$ increases slightly for the graphite electrodes type EDM-3, remaining almost constant for electrodes made of graphite HK-6.

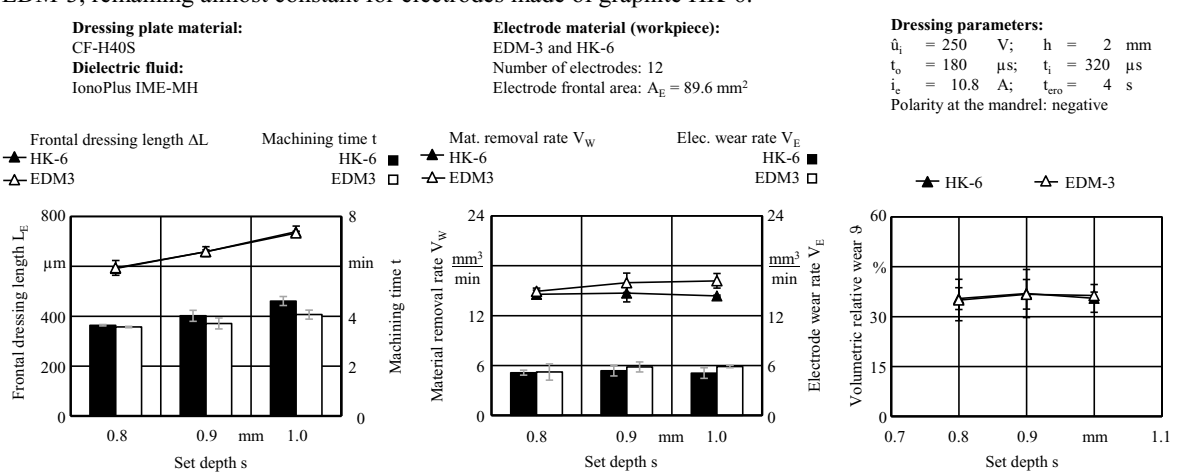


Fig. 5. Influence of workpiece material on the dressing results applying graphite cemented carbide CF-H40S as dressing plate.

The material removal rate $V_W$ is higher and the machining time t is shorter while dressing the graphite electrodes made of EDM-3 in comparison to HK-6. This relies on the difference of grain size between both materials and on the material removal mechanisms during the EDM applying graphite electrodes. The volumetric relative wear ϑ for EDM-3 and HK-6 remains almost constant with increasing machining depth s, with very similar values for both materials. This is a result of a constant material removal rate $V_W$ and a constant electrode wear rate $V_E$ while dressing HK-6, while both values slightly increase while dressing the graphite EDM-3. A machining depth s = 0.9 mm was chosen for both electrode materials EDM-3 and HK-6 during the integration of the dressing technology into an automated production cycle applying a dressing plate made of cemented carbide CF-H40S. The dressing technology enabled the fulfillment of all requirements while applying the tool electrodes EDM-3, with a material removal rate $V_W$ = 15.95 mm³/min, a frontal dressing length $L_E$ = 658.9 µm and a machining time t = 3.71 min. For the graphite electrodes made of the material HK-6, a material removal rate $V_W$ = 14.7 mm³/min, a machining time t = 4.02 min and a frontal dressing length $L_E$ = 658.3 µm were achieved.

## 4. Integration of the dressing technology into the process chain

The implementation of the dressing technology with the dressing plate fixed to the machine tool was carried out with dressing plate material cemented carbide CF-H40S, and for the two distinct graphite electrode materials tested, namely EDM-3 and HK-6. Fig. 6 shows the experimental set-up for the integration of the dressing technology into the process chain. A total of 12 graphite electrodes, totalizing an electrode frontal area of $A_E$ = 89.6 mm², are dressed simultaneously and are subsequently applied for producing 12 seal slots in the workpiece made of nickel-base casting alloy MAR-M247. The schematic representation of both dressing and EDM presented in Fig. 2 also helps understanding the experimental procedure applied.

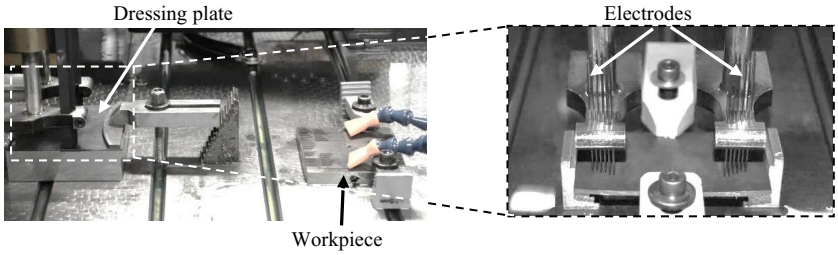


Fig. 6. Experimental set-up for the integration of the dressing technology into the process chain.

The seal slots are produced in the workpiece by means of the EDM and the tool electrodes present a worn profile after this step. Afterwards, the dressing process starts on the dressing plate and, subsequently, the tool electrodes present a renewed profile. The EDM process starts over again and this automated production cycle is repeated continuously for the machining of the slots in MAR-M247. The analysis of results comprised the measurement of the radius of electrodes after machining and dressing, of the radiuses inside the cavities, of the surface roughness of cavities, and finally a metallographic analysis of the sub-surface applying the SEM. Fig. 7 presents the process results both for EDM (top) of slots as well as for dressing of tool electrodes (bottom). The material removal rate $V_W$ during the EDM of seal slots is higher for the graphite electrodes HK-6 than for the electrodes EDM-3, with $V_{W(HK-6)}$ = 49.4 mm³/min and $V_{W(EDM-3)}$ = 32.6 mm³/min, respectively. This is a result of the lower specific electrical resistance ρ of HK-6, combined with the smaller primary grain size of this graphite, resulting in better process behavior and less buildup of remelted material on the electrode. The volumetric relative wear ϑ is higher for EDM-3 than for HK-6 electrodes, due to the bigger primary grain size of the graphite EDM-3 and the known wear mechanism of graphite electrodes [12] during EDM. As the material removal mechanism of graphite during EDM consists on the sublimation of the bonding material that was graphitized during the graphitization, thereby breaking off the whole primary grains of the bond, the higher grain size of EDM-3 electrode leads to higher volumetric relative wear ϑ. Regarding the dressing technology, the frontal dressing length $L_E$ achieved for all electrode materials tested are in accordance with the boundary conditions for the dressing technology, with 600 µm < $L_E$ < 800 µm. The material removal rate $V_W$ during the dressing process is higher while dressing the

EDM-3 electrodes due to the higher grain size of this material and again due to the material removal mechanism of graphite during EDM previously explained.

**EDM-machining of seal slots:**
s = 11 mm; $\hat{u}_i$ = 270 V
$i_e$ = 29 A; $t_0$ = 14 µs
$t_i$ = 32 µs
Polarity of the graphite electrodes: positive
**Variable parameters in function of the depth:**

| Depth [mm] | 0 - 7.5 | 7.5 - 11 |
|---|---|---|
| $t_{ero}$ [s] | 6.4 | 0.5 |
| h [mm] | 7.5 | 4.0 |

**Dressing of electrodes:**
s = 0.9 mm
$\hat{u}_i$ = 250 V
$i_e$ = 10.8 A
h = 2 mm
$t_{ero}$ = 4 s
$t_0$ = 180 µs
$t_i$ = 320 µs
Polarity of the graphite electrodes: negative

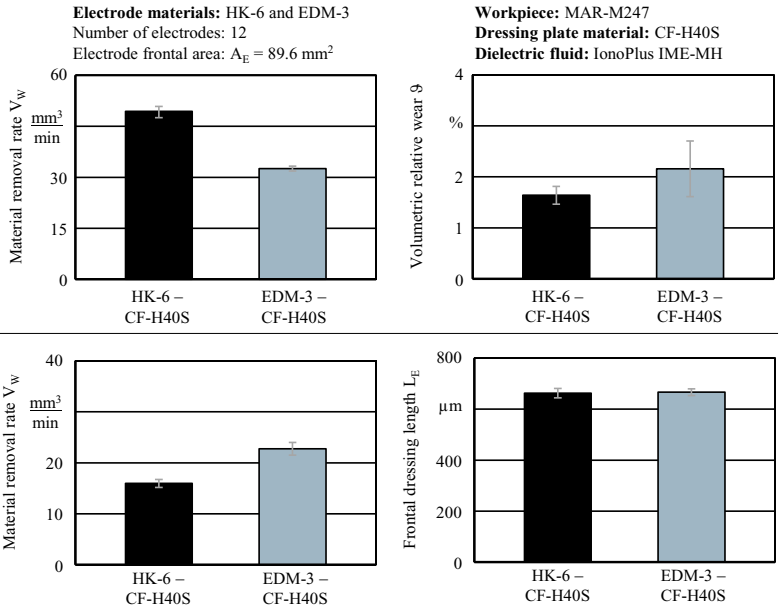


Fig. 7. Process results for the EDM of seal slots and dressing of distinct tool electrodes applying dressing plate material CF-H40S.

The following analysis focused on the measurement of the corner radius of electrodes $R_E$ and on the corner radius of produced cavities $R_C$ with increasing number of dressing cycles. The Fig. 8 (left) clearly shows the difference of the corner radius of electrodes $R_E$ after the EDM of successive set of cavities in alloy MAR-M247, with and without the application of the dressing technology. The electrode corner radius $R_E$ increases uninterruptedly with increasing number of cycles, if these electrodes are not dressed between the EDM cycles, while the radiuses of tool electrodes $R_E$ that went through the dressing maintained almost constant values with increasing number of EDM cycles.

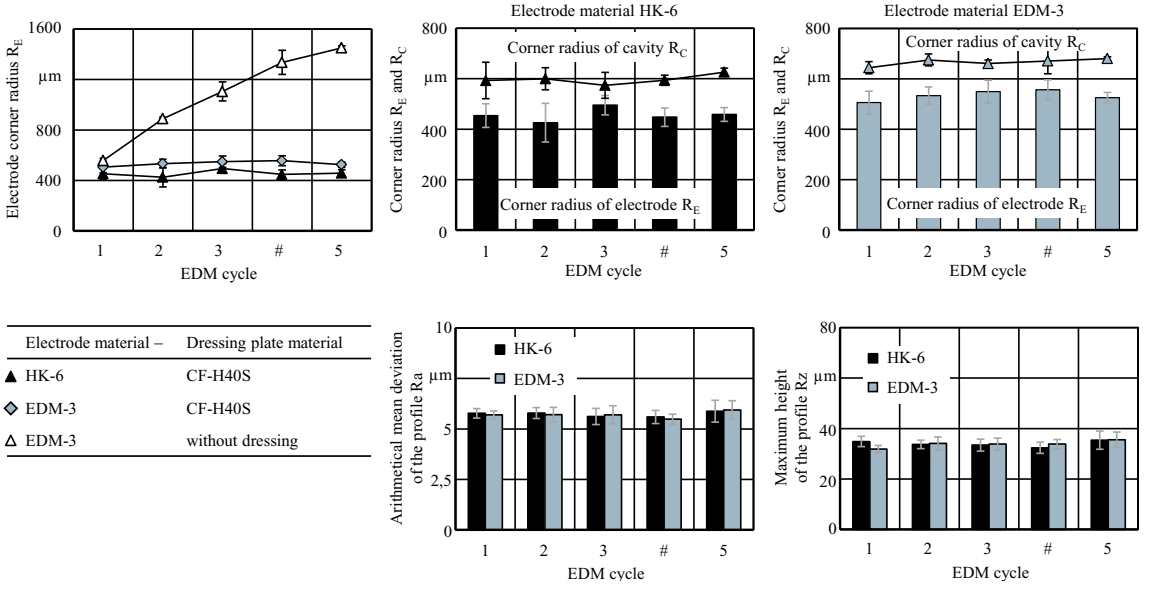


| Electrode material – | Dressing plate material |
|---|---|
| ▲ HK-6 | CF-H40S |
| ◆ EDM-3 | CF-H40S |
| △ EDM-3 | without dressing |

Fig. 8. Corner radius of electrodes $R_E$, corner radius of cavities $R_C$ and surface roughness of seal slots Ra and Rz.

The two remaining upper diagrams show the corner radius of electrode $R_E$ and of cavity $R_C$ both for HK-6 and EDM-3 with increasing number of EDM cycles. It is clear that both $R_E$ and $R_C$ remain almost constant with increasing number of cycles, being the radius of cavities $R_C$ a function of the radius of electrodes $R_E$ and of the machining gap. $R_C$ is also always below the required tolerance $R_C < 1$ mm. The corner radiuses of produced cavities $R_C$ applying the electrodes EDM-3 are higher than the radiuses applying the HK-6 electrodes, as a consequence of higher volumetric relative wear of EDM-3 during EDM. These results also confirm that the electrode materials that exhibit less relative wear during the die-sinking EDM process enable the production of more precise cavities in the workpieces. The values for the arithmetical mean deviation of the profile Ra and the maximum height of the profile Rz remain constant during all five EDM cycles and the values are very similar for both electrode materials, meaning that the dressing process has no influence on the surface roughness of produced cavities. The SEM-images, which are not presented here, also showed no influence of the dressing technology on the surface integrity of parts.

## 5. Conclusions

The development of the dressing technology was carried out in this work, with the analysis of four distinct dressing plate materials. The results presented focused on the application of fine grained cemented carbide CF-H40S as dressing plate. The statistical analysis showed that the parameters erosion time between flushing intervals $t_{ero}$ and discharge current $i_e$ possessed a high significant influence on at least one process output, being thus applied in the full-factorial optimization. The full-factorial analysis enabled the choice of the optimized electrical parameters prior to the integration of the dressing technology into the process chain. The integrated technology enabled the fulfillment of technological boundary conditions set on the process, including minimal material removal rate $V_{W,min} = 13.44$ mm$^3$/min and frontal dressing length $L_E > 600$ µm. The radii both of tool electrode $R_E$ as well as of the produced cavities $R_C$ remain constant with increasing number of produced cavities, with $R_C$ within the required tolerances set by the OEMs ($R_C < 1$ mm), guaranteeing therefore the form accuracy of seal slots. The dressing technology has nearly no influence on the subsequently EDM process regarding both the surface roughness and the surface integrity of the parts. The dressing technology proved to be an alternative during the production of seal slots in turbine components, and may lead to a fully automation of the EDM of these features. The manipulation by the operator can be reduced or eliminated, reducing the set-up times and finally achieving full process automation.

## References

[1] K. Steffens, H. Wilhelm: Next engine generation: Materials, Surface Technology, Manufacturing Processes – What comes after 2000? URL: http://www.mtu.de (access 02/2016).
[2] K. Steffens, A. Schäffler: Advanced Compressor Technology – Key Success Factor for Competitiveness in modern Aero Engines, information on http://www.mtu.de (access 02/2016).
[3] E. Uhlmann, D.C. Domingos (2013): Investigations on Vibration-Assisted EDM-Machining of Seal Slots in High-Temperature Resistant Materials for Turbine Components. Procedia CIRP 6:71-76.
[4] Uhlmann, E.; Domingos, D. C. (2013): Development and Optimization of the Die-Sinking EDM-Technology for Machining the Nickel-Based Alloy MAR-M247for Turbine Components. Procedia CIRP 6:181-186.
[5] E. Uhlmann, D. C. Domingos (2016): Investigations on Vibration-assisted EDM-machining of Seal Slots in High-Temperature Resistant Materials for Turbine Components - Part II. Procedia CIRP 42:334-339.
[6] F. Klocke, A. Klink, D. Veselovac, D. K. Aspinwall, S. L. Soo, M. Schmidt, J. Schilp, G. Levy, J.-P. Kruth (2014): Turbomachinery component manufacture by application of electrochemical, electrophysical and photonic processes. CIRP Annals - Manufacturing Technology 63(2), pp. 703-726.
[7] POCO GRAPHITE INC: Technical Manual. Texas, USA. Corporate Literature. 2014. URL: http://edmtechman.com/about.cfm (access 03/2016).
[8] TOKAI CARBON DEUTSCHLAND GMBH: Funkenerosion Graphit-Marke HK-6. Material data-sheet. 2014.
[9] DONCASTERS PRECISION: Verification certificate for material MARM247, according to DIN EN 10204 3.1. Bochum, 2013.
[10] J. R. Kattus: Aerospace Structural Metals Handbook, code 4218, p.1-8, Purdue Research Foundation, West Lafayette, Indiana, 1999.
[11] F. Klocke: Theoretische Modelle zur Funkenerosion - Grundlagenuntersuchungen an elektrischen Entladungen unter flüssigen Dielektrika. Abschlussbericht zum Forschungsvorhaben Kl 500/23-1. 2002.
[12] A. Karden: Funkenerosive Senkbearbeitung mit leistungssteigernden Elektrodenwerkstoffen und Arbeitsmedien. Bericht aus der Produktionstechnik. Hrsg.: Klocke, F. Aachen: Shaker, 2001.